

VISUALIZING SOFT MATTER: MESOSCOPIC SIMULATIONS OF MEMBRANES, VESICLES AND NANOPARTICLES

JULIAN SHILLCOCK* and REINHARD LIPOWSKY

*Theory Department,
Max Planck Institute of Colloids and Interfaces,
14424 Potsdam, Germany
Julian.Shillcock@mpikg.mpg.de

Received 27 September 2006

Revised 22 December 2006

Biological membranes have properties and behavior that emerge from the propagation of the molecular characteristics of their components across many scales. Artificial smart materials, such as drug delivery vehicles and nanoparticles, often rely on modifying naturally-occurring soft matter, such as polymers and lipid vesicles, so that they possess useful behavior. Mesoscopic simulations allow *in silico* experiments to be easily and cheaply performed on complex, soft materials requiring as input only the molecular structure of the constituents at a coarse-grained level. They can therefore act as a guide to experimenters prior to performing costly assays. Additionally, mesoscopic simulations provide the only currently feasible window on the length and time scales relevant to important biophysical processes such as vesicle fusion. We describe here recent work using Dissipative Particle Dynamics simulations to explore the structure and behavior of amphiphilic membranes, the fusion of vesicles, and the interactions between rigid nanoparticles and soft surfaces.

Keywords: Dissipative particle dynamics; simulations; lipid membranes; vesicle fusion; nanoparticles.

1. Introduction

Computer simulations have been used to study the properties of small amounts of matter for more than 50 years, but it is only in the last decade or so that such simulations have been able to approach the length and time scales relevant to biological processes. The Molecular Dynamics (MD) technique was first used to study the properties of a set of hard disks¹ by integrating Newton's equations of motion. The Monte Carlo (MC) technique² was invented to calculate thermodynamic properties of matter, such as the equation of state. Even as MD simulations have become more applicable to experimental systems with the development of increasingly accurate, and complex, force fields, they remain limited to nanometer length scales by the computational demand of calculating the interactions amongst all the particles. For biological systems that are immersed in aqueous solvent, reaching beyond tens

of nanometers and a few microseconds requires the use of prohibitively-expensive supercomputers.

Such restrictions have driven the development of coarse-grained, or *mesoscopic*, simulations that are able to follow the dynamical behavior of micron-sized amounts of matter for microseconds and, sometimes, milliseconds. By attempting to keep only those molecular details that are expected to be essential in determining the long length- and time-scale properties of a system, mesoscopic simulations are able to represent dynamical phenomena in systems that are visible in the light microscope. This provides fascinating glimpses into the complex, dynamic life of cells, but also gives us the ability to model and visualize the properties of artificial materials, such as vesicles and nanoparticles, an ability that is becoming increasingly important in the development of new drugs,³ drug delivery systems,⁴ and semiconductor nanomaterials.⁵ A wide variety of mesoscopic simulation techniques⁶ have been developed to reveal the dynamics of biophysical processes, and they each have their strengths and weaknesses. This article describes the application of one particular mesoscopic technique, Dissipative Particle Dynamics^{7,8} (DPD), to the problems of creating a semi-quantitative model of naturally-occurring phospholipid membranes^{9–12} and artificial polymeric vesicles¹³; the fusion of a vesicle with a larger membrane¹⁴; and the interaction of rigid nanoparticles with soft membranes. This choice of problems reflects the authors' belief that modeling soft materials, such as lipid membranes, and gradually adding dynamical capabilities to the model, such as the fusion of vesicles, is a promising route towards constructing increasingly accurate *in silico* cell models. When these models have been sufficiently developed, they can be used to generate hypotheses that can be subsequently checked in experimental assays. The ability to map data obtained from multiple experimental techniques onto molecular components within a unified simulation model is also a crucial integrative function of such simulations.

Experimental techniques for visualizing the structure and behavior of living cells have revealed more and more details in recent years. Fluorescence microscopy and fluorescence resonant energy transfer (FRET) in particular now allow the motion and interactions of single molecules within living cells to be observed and followed in time. This has resulted in a huge flow of experimental data on the concentration, and interactions between, for example, the protein and lipid components within cells under specific conditions. Making sense of these data sets, especially when trying to integrate results from distinct experimental protocols, is very difficult. Computer models of cellular processes could be used to make predictions about the consequences of varying key parameters in the model, with a speed and precision that is often experimentally impossible due to inextricable couplings between different components in the system. In order to achieve this goal, the model must contain enough complexity to allow it to reproduce the experimental observations, but also be simple enough to yield insights that cannot be obtained simply by data-mining the experimental results. Dynamical processes in a cell, such as synaptic vesicle transport to the plasma membrane and

its subsequent fusion, represent valuable model systems for testing the utility of computer models.

Advances in understanding the structure and function of cellular components has led to an increasing desire to modify or create from scratch supramolecular systems that can perform therapeutic functions.¹⁵ Examples include targetting¹⁶ tumor cells with toxic payloads¹⁷ while leaving surrounding (healthy) cells unaffected, and delivering healthy genes to replace defective ones using polymers.¹⁸ A key step towards developing these systems is being able to rationally modify the properties of complex molecular aggregates, including liposomal¹⁹ and polymeric²⁰ vesicles, and rigid nanoparticles dubbed artificial viruses.⁴ As such systems often have dimensions up to a few hundred nanometers, this means that they are ideal candidates for being studied using a mesoscopic simulation technique. Nanoparticles may be given a layered structure^{21,22}, in which each layer is composed of a different material and serves a specific role in the process of transporting the drug payload to the target cells.⁴ Even simple questions such as the effects of size variation on the properties of the nanoparticles can be hard to answer experimentally unless precise control over the construction process is obtained. Simulations of amphiphilic membranes, vesicles and nanoparticles are relatively simple to perform compared to their experimental counterparts. Such simulations can therefore act as a search-light to explore the huge parameter space for complex aggregates, and pose questions to which subsequent experiments can give definitive answers. In order to capture in a simulation the behavior of typical nanoparticles in cellular environments, a minimum set of supramolecular entities is required. These include: membranes of varying composition and physical properties; rigid particles or shells that can encapsulate bulk fluid; hydrophobic, hydrophilic or amphiphilic polymers. Additionally, it is important to be able to modify the properties of the simulated aggregates embedded within the surrounding fluid environment so as to mimic, for example, the effects of pH, the response of a polymer species to a good or bad solvent, or cytoplasmic crowding of molecular species.

In the remainder of this article, we give an overview of the DPD technique, describe some recently-published applications to biophysical systems, and conclude with our vision of using a combination of mesoscopic simulation techniques to model a cell signaling network. Such a model could be used to test hypotheses relating to the design of artificial materials and nanoparticles for therapeutic intervention.

2. Coarse-grained Modeling of Complex Fluids: The DPD Approach

Dissipative Particle Dynamics is a particle-based, explicit-solvent simulation technique that was created for the simulation of fluids at larger length and time scales than is possible using atomistic Molecular Dynamics, whilst retaining the hydrodynamic modes that are missing in techniques such as Monte Carlo and Brownian Dynamics.

The original DPD algorithm of Hoogerbrugge and Koelman⁷ had some deficiencies that were removed by later workers,^{8,23} and it is the Groot-Warren version²³ of the DPD integration scheme that is now most commonly used. An early review of the technique was published by Warren²⁴, and a comparison of various methods of simulating surfactant solutions followed.²⁵ A detailed analysis of DPD simulations of phospholipid systems has been published recently.²⁶ Early applications of the DPD technique included microphase separation of polymeric mixtures,²⁷ the dynamics of an oil droplet near a hard surface in shear flow,²⁸ aggregation of surfactants onto a polymer in a bulk surfactant solution,²⁹ colloidal motion in a solvent,³⁰ and rupture of a planar membrane patch by incorporation of nonionic surfactants.³¹ It was also applied to the packing of surfactants at an oil-water interface and their efficiency at reducing the surface tension,³² following the evolution of the interface between pure surfactant and water³³ and the behavior of grafted polymer brushes subject to shear flow.³⁴

The Dissipative Particle Dynamics simulation algorithm⁷ defines small *fluid elements* as its fundamental units. This makes it distinct from classical Molecular Dynamics which uses atoms and molecules. The volume elements, which are often referred to as *beads*, are assumed to contain a number of molecules or molecular groups. A solvent bead in a DPD simulation of an amphiphilic membrane in water typically represents between 3 and 10 water molecules.³¹ The exact mapping from one bead to a number of molecules depends on the molecular nature of the material the bead is to represent.¹³ The physical masses of all beads (m) in a DPD simulation are usually assumed to be identical, as are their sizes (d_0). Note that this length d_0 is the distance at which all non-bonded, bead-bead forces vanish, and it corresponds to the *diameter* of a bead if one pictures two beads at the extreme of their interaction range as two spheres whose surfaces just touch. The remaining physical unit required to convert from dimensionless simulation quantities to physical quantities is a time-scale (or, equivalently, an energy scale). This can be extracted from the time-scale of a relevant process in the simulated system. For the simulation of fluid amphiphilic membranes and vesicles, it is common to use the amphiphiles' in-plane diffusion coefficient to set the time-scale. This is obtained by calculating the average of the mean-square displacement of all the molecules in a membrane, and taking the ratio of its long-time limiting value to the elapsed time as a measure of the diffusion coefficient. This is not the only choice, however, and the time-scale associated with a simulated process may depend on details of the DPD implementation.³⁵

Once the beads are defined, they must interact. The forces between beads in a DPD simulation are *effective* forces that are chosen so that they locally conserve mass and momentum and are pairwise additive. These conservation laws, together with the fact that the total force on a bead is the sum of all the forces due to its neighbors within a fixed distance, ensure that hydrodynamic interactions emerge in a DPD fluid for much smaller particle numbers and on shorter time-scales than is possible in MD simulations.

The total force between two beads in the fluid is the sum of three contributions. The first type of force is a conservative interaction that corresponds in purpose, although not in its functional form, to the Lennard-Jones interaction between two atoms in an MD simulation. It allows beads to be given an identity, so that a water bead and an oil bead feel a mutual repulsion that leads to phase separation. The magnitude of the conservative force is related to the compressibility of the fluid being simulated.²³ The other two forces are a random and a dissipative force that together constitute a thermostat that adds energy to the fluid and extracts energy from the fluid respectively. Unlike the thermostats commonly used in MD simulations (for a comparison of their properties see Stoyanov and Groot³⁵ and Soddemann *et al.*³⁶), the DPD thermostat conserves momentum locally, and it is this that allows the hydrodynamic interactions in the fluid to propagate. To maintain the fluid at a pre-set temperature, the magnitudes and functional forms of the thermostat forces have to be chosen appropriately; when this is done, they satisfy a fluctuation-dissipation theorem, and the equilibrium states of the fluid are generated with a probability that obeys the Boltzmann distribution. All three forces are soft and short-ranged, vanishing beyond the cut-off distance d_0 .

As DPD has become more widely used, attempts have been made to improve the scheme's thermostat, which has been shown^{37–39} to lead to spurious results if too large a time-step is used in the integration scheme. These include changing the type of thermostat^{40,41} to improve the temperature control,⁴² and combining two different thermostats,³⁵ and randomly selecting one or the other for each interacting particle pair, that allows the viscosity of a DPD fluid to be varied by orders of magnitude. The DPD thermostat can also be applied to other particle-based simulation techniques.³⁶ Other changes have included simulations in the constant pressure and constant surface tension ensemble,³⁹ and the replacement of the original potentials with density-dependent ones that include an attractive part thereby allowing liquid-gas interfaces to appear in the simulations,⁴³ a process that is forbidden in the original algorithm by the quadratic nature of the DPD fluid's equation of state.

The state of the fluid is evolved in time by integrating Newton's equations of motion for all the beads in the system. Because the thermostat involves a stochastic term (in the random force) and a velocity-dependent term (in the dissipative force), the choice of integrator is not as simple as for MD simulations that contain (velocity-independent) Lennard-Jones interactions. A variety of integration schemes have been proposed^{40,42,44} to reduce artifacts due to the step size and to handle the thermostat force appropriately, but the most commonly-implemented one, which has been shown³⁸ to be as good as more complicated schemes if the integration time-step is chosen small enough, is a modified Velocity-Verlet scheme introduced by Groot and Warren.²³ For more details of the scheme, the reader is referred to their original paper.

We note here that temperature enters into the DPD formulation in two ways. First, the average kinetic energy of the beads defines the *kinetic* temperature; and, second, the ratio of the random force parameter to the dissipative force parameter

defines the *thermostat* temperature. These should be the same for any simulation, but if the integration scheme is not chosen carefully, or the integration step size is chosen too large, the kinetic and thermostat temperatures may diverge. This leads to the somewhat surprising result that the kinetic temperatures of different bead types may be different in the same simulation. These artifacts have recently⁴⁵ been extensively investigated, and are related to the use of too large an integration step-size. For concreteness, we have found that an integration step of 0.02 (in DPD time units of $\sqrt{md_0^2/k_B T}$) is usually appropriate for lipid membrane simulations, although an even smaller value may be necessary if stiff Hookean springs are used within molecules.

The forms of soft matter we consider here are composed of *amphiphilic* molecules such as phospholipids and diblock copolymers. Amphiphiles contain a hydrophilic piece chemically bonded to a hydrophobic piece. Phospholipids come in many shapes and sizes, and may possess one, two or more hydrocarbon tails, and have a charged, polar or neutral headgroup with a variable degree of bulkiness. Diblock copolymers are typically long-chain polymers composed of a mixture of hydrophilic and hydrophobic monomers. Goetz and Lipowsky⁴⁶ introduced a simple model phospholipid architecture consisting of three hydrophilic beads (designated H) to which are attached two linear hydrophobic tails each containing four chain beads (C). Such an amphiphile is represented as $H_3(C_4)_2$. A representative diblock copolymer composed of similar monomer types could be $H_{24}C_{40}$, in which 24 hydrophilic monomers are connected in a linear chain to 40 hydrophobic monomers. The amphiphiles are contained within an aqueous solvent (W). Each solvent bead represents a volume of water consisting of several molecules. Because the solvent beads have a length scale of the order of 1 nm, there are no explicit hydrogen bonds. Their effects are subsumed in the conservative interaction parameters between the solvent beads and the hydrophilic and hydrophobic beads. The functional forms of the various non-bonded and bonded forces between all bead types is given next.

The conservative force between two beads i, j separated by a distance r_{ij} is

$$F_{ij}^C = a_{ij} (1 - r_{ij}/d_0) \hat{r}_{ij} \quad (1)$$

for $r_{ij} < d_0$, and zero otherwise. The range of the force is set by d_0 , and a_{ij} is the maximum force between beads of types i, j ; r_{ij} is the distance between the centres of beads i, j , and \hat{r}_{ij} is the unit vector pointing from bead j to bead i . Note that the conservative force is always finite, taking its maximum value, a_{ij} , at zero separation.

The dissipative force between two beads is linear in their relative momenta and takes the form

$$F_{ij}^D = -\gamma_{ij} (1 - r_{ij}/d_0)^2 (\hat{r}_{ij} \cdot v_{ij}) \hat{r}_{ij} \quad (2)$$

where γ_{ij} is the strength of the dissipation between beads i, j , and $v_{ij} = v_i - v_j$ is their relative velocity (which is the same as their momentum as we measure all masses in units of the mass scale m in our simulations).

Finally, the random force between a bead pair is

$$F_{ij}^R = \sqrt{2 \gamma_{ij} k_B T} (1 - r_{ij}/d_0) \zeta_{ij} \hat{r}_{ij} \quad (3)$$

where values of the random force are generated by sampling a uniformly-distributed random variable, $\zeta_{ij}(t)$, that satisfies $\langle \zeta_{ij}(t) \rangle = 0$ and $\langle \zeta_{ij}(t) \zeta_{i'j'}(t') \rangle = (\delta_{ii'} \delta_{jj'} + \delta_{ij'} \delta_{ji'}) \delta(t - t')$. The random force has the symmetry property $\zeta_{ij}(t) = \zeta_{ji}(t)$ that ensures local momentum conservation, and hence the correct hydrodynamic behavior of the simulated fluid on long length scales. Note that we have replaced the (nominally-independent) random force parameter σ_{ij} by its value as determined from the fluctuation-dissipation relation $\sigma_{ij}^2 = 2 \gamma_{ij} k_B T$ as shown by Groot and Warren.²³

Molecules are constructed by tying beads together using Hookean springs with the potential

$$U_2(i, i+1) = \frac{1}{2} k_2 (r_{ii+1} - l_0)^2 \quad (4)$$

where $i, i+1$ label adjacent beads in the molecule. The spring constant, k_2 , and unstretched length, l_0 , are chosen so as to fix the average bond length to a desired value. Both parameters may be specified independently for each bead type pair allowing a linear chain's bond strength to vary along its length.

Chain stiffness is modeled by a three-body potential acting between adjacent bead triples in a chain,

$$U_3(i-1, i, i+1) = k_3 (1 - \cos(\phi - \phi_0)) \quad (5)$$

where the angle ϕ is defined by the scalar product of the two bonds connecting the pairs of adjacent beads $i-1, i$ and $i, i+1$. In general, the bending constant, k_3 , and preferred angle, ϕ_0 , may be specified independently for different bead type triples allowing the chain stiffness to vary along a molecule's length. A preferred angle of zero means that the potential minimum occurs for parallel bonds in a chain.

3. Membranes, Vesicles and Polymersomes: Material Properties

Several groups have used DPD to simulate the formation⁴⁷ and equilibrium properties of amphiphilic bilayer membranes, including the lateral stress profile,⁹ and the effects of various amphiphile architectures on membrane material properties.^{10–12} This has extended previous work that used coarse-grained Molecular Dynamics simulations to measure the surface tension⁴⁷ and bending rigidity^{46,48} of planar bilayer patches. The advantage of DPD over MD for these systems is that membranes containing tens of thousands of lipid molecules can be simulated using a few days of CPU time. This allows good statistics to be collected on membrane observables.

These simulations have been extended to more complex systems, such as nanospheres in multicomponent fluids⁴⁹ and the fusion of tense vesicles to planar membranes.¹⁴ The range of soft matter systems now being studied by DPD

includes vesicles formed of diblock copolymers,¹³ called *polymersomes*, blends of homopolymers and diblock copolymers,⁵⁰ the aggregation of copolymer analogues of the exon1 fragment of the protein Huntingtin that is involved in Huntington's disease driven by the relative hydrophobicity of different regions of the fragment,⁵¹ the behavior of a worm-like chain model of DNA polymers,⁵² and the influence of model proteins embedded in a fluid membrane.⁵³

Planar amphiphilic membranes in aqueous solvent tend to close into vesicles, and DPD has been used to follow vesicle formation,⁵⁴ and the budding¹² and fission of two-component vesicles.^{55,56} A recent review⁵⁷ of the self-assembly of vesicles and liposomes shows that it is a generic behavior of many different types of molecule, and some of the resulting aggregates have exciting properties for medicinal and pharmaceutical applications. Diblock copolymers are an example of a non-lipidic class of bilayer and vesicle forming molecule.^{58,59} Each molecule consists of a hydrophilic block, containing water-soluble monomers, chemically bonded to a hydrophobic block, containing water-insoluble monomers. The properties of the polymers, and the aggregates they form, depend on the relative lengths of the two blocks, the molecular weight of the polymer, and the presence of functional groups attached to side chains. A typical example of this class of polymer is poly(ethylene-oxide)-polyethylene (PEO-PEE). The size of each block can be varied from a few monomers up to hundreds of monomers.

Polymersomes have physical properties, such as the membrane thickness and elastic moduli, that span a wider range of values⁵⁹ than lipid vesicles, and can be designed to automatically degrade under given conditions.^{60,61} This makes them attractive as drug delivery vehicles because they are not recognised by a patients' immune system. The interior structure of the membrane of a polymersome differs substantially from that of a phospholipid membrane. Figure 1 shows a snapshot taken at 600 ns from an equilibrated system containing both a polymersome and a lipid vesicle with comparable diameters of about 30 nm immersed in a solvent. The solvent particles are invisible for clarity. The membrane thickness and character of the inner and outer surfaces are quite distinct. The hydrophobic block of the polymersome is sequestered between the well-hydrated hydrophilic blocks, and the aqueous solvent penetrates to the edge of the hydrophobic region. The entanglement of the individual molecules leads to slow inplane diffusion, and a greater resistance to rupture under lateral stress. By contrast, the vesicle membrane is about one half the thickness of the polymersome's membrane, and its surface is quite smooth. It also shows a greater degree of thickness variation than the polymersome. These vesicles are similar in size to synaptic vesicles in neurons, and show that DPD can capture the behavior of quite distinct aggregates. Recent experiments⁶² have explored the interactions of short, amphipathic peptides, such as alamethicin, with (uncharged) diblock copolymer membranes and found that even though the peptides are less than one half of the membrane width they permeabilize it quite effectively. Other experiments using 50 micron diameter polymer vesicles⁶³ have shown that they undergo fusion when subject to ultrasound. Molecularly-detailed

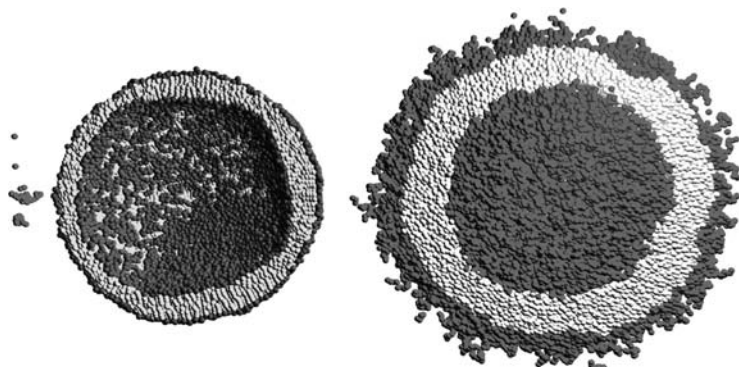


Fig. 1. Snapshot of a system containing both a model lipid vesicle and polymersome with diameters approximately 30 nm in bulk solvent. The polymersome contains 2616 diblocks with the architecture $H_{29}I_{T_{47}}$. The vesicle contains 5887 lipids with architecture $H_3(T_4)_2$. The simulation box has size $56 \times 56 \times 84 \text{ nm}^3$, and contains approximately 2.3 million beads of all types. For clarity, the solvent particles, which fill the inside and outside of the vesicle and polymersome, are invisible. For more details on the interaction parameters for the hydrophilic and hydrophobic monomers of the diblocks¹³ and the head and tail beads of the lipids¹⁴ the reader is referred to the literature. The bead type I connects the hydrophilic and hydrophobic blocks of the diblocks, and has interaction parameters similar to those of the hydrophobic monomers. The contrast between the smooth lipid vesicle membrane and the thicker, rough polymersome membrane is evident. The hydrophilic blocks of the copolymers are well hydrated and extend into the solvent phase, while their hydrophobic blocks are compressed between them. The surface of the lipid vesicle is smooth because the small lipid headgroups are pressed against the hydrophobic tails shielding them from the solvent. The width of the polymersome membrane, around 6 nm, is approximately twice that of the vesicle membrane. (The beads visible at the extreme left of the image belong to diblocks in the polymersome that are wrapped around because of the periodic boundary conditions in the simulation box. Image produced using the PovRay ray tracing program: www.povray.org.)

simulations of the fusion of two polymersomes would be valuable for exploring the molecular architectural space of polymersomes, and for optimizing their physico-chemical properties for clinical applications.

Unfortunately, the high molecular weight of some diblock copolymers, and the large diameter of polymersomes, currently restricts atomistic MD simulations to a few tens of molecules, and even coarse-grained MD simulations are limited to patches of a hundred or so molecules.⁶⁴ These limitations, and the soft nature of polymer vesicles, makes them a prime target for DPD modeling. The variation in polymersome physical properties with the molecular weight of the constituent molecules forms an important link between experimental results, analytical theories and simulations. Ortiz *et al.* have performed DPD simulations¹³ of membrane patches of diblock copolymers of various molecular weights, calibrating the DPD parameters using data obtained from atomistic MD simulations of the same system.

Typically, every bead of each molecular species in a multi-component DPD simulation is considered to contain the same amount of matter, and the self-interaction parameters are chosen so that the compressibility of each pure species matches that of water at room temperature. The cross-terms are then matched to the relative

solubility of each species in the others. For species that are mutually soluble, such as the PEO block and water relevant for polymersome simulations, a different property has to be chosen. Ortiz *et al.* choose the radial distribution function of PEO in water for this purpose.¹³ Using the conventional DPD mapping for simulations of a planar membrane patch of diblocks, they find that the geometry of the hydrophobic block is incorrect and the hydrophobic density is too high. This leads to unphysical values for the membrane area stretch modulus. A revised mapping was developed in which the beads of each species are considered to contain an amount of matter that depends on the species, and is chosen so as to reproduce the experimental bulk density. For the PEO-PEE diblock considered this leads to the density-based mapping of 1.392 PEO monomers/bead, 0.774 PEE monomer/bead and 3.01 water molecules/bead. This is in contrast to the conventional mapping in which the first two ratios are unity.

Using the new mapping, the membrane area stretch modulus is found to be 137 mN/m, which is in good agreement with the experimental value⁵⁹ of 120 ± 20 mN/m. Additionally, the scaling of the membrane hydrophobic block thickness with polymer molecular weight was found to obey the experimentally-observed scaling law $d \sim M^{1/2}$. Neither of these results were obtained using the conventional DPD mapping. The new DPD mapping¹³ was used to simulate the rupture of a 28 nm diameter polymersome containing 1569 diblock copolymers after being inflated with excess internal solvent. The first step in the rupture pathway appears to be micellization of the inner leaflet which subsequently weakens the outer leaflet allowing the solvent to escape via multiple pores.

4. Vesicle Fusion

Vesicle fusion has been estimated to require tens of milliseconds in laboratory experiments,^{65,66} and *in vivo* experiments suggest it may require hundreds of microseconds.⁶⁷ Very recently, the controlled fusion of vesicles driven by either electroporation or the interactions of fusogenic molecules embedded in the vesicle membranes has been visualized⁶⁸ using a fast digital camera with a temporal resolution of 50 μ s. The relevant length scales range from less than a nanometer for the initial fusion pore width up to tens of microns for the vesicle diameter. Several reviews^{69–72} of experimental fusion processes and theoretical models have appeared in the last few years, including two recent ones.^{73,74} Although fusion of giant (1–20 micron diameter) vesicles can be observed using video microscopy,⁶⁸ fluorescence microscopy⁷⁵ and optical dark-field microscopy,⁷⁶ and SNARE-mediated fusion of liposomes to a supported planar membrane has been followed using total internal reflection fluorescence microscopy,⁷⁷ the molecular rearrangements that take place during the final stage of the fusion process, when the two initially-distinct membranes join and produce a fusion pore, cannot yet be resolved by these experimental techniques.

The length and time scales of vesicle fusion render the use of atomistic MD simulations computationally demanding, and even coarse-grained MD simulations are restricted to small systems. This is due to the twin requirements of having to simulate the motion of every atom in the system and needing a small (femtosecond) integration time step. The soft potentials of DPD, which contain no hard core as do the Lennard-Jones potentials typically used in MD simulations, together with the grouping of several atoms or atomic groups into one DPD bead, allows vesicle fusion events to be simulated for times that approach the experimental range. The steady increase in computer processing speeds has allowed the more quantitative method of coarse-grained MD to match DPD in the simulation time-scale, but it is still restricted to smaller length-scales. We compare here the application of various simulation techniques to the fusion of lipid membranes. Coarse-grained MD simulations have been used by several groups to explore the fusion of two 15 nm vesicles, containing about 1000 lipids each.^{78–80} These studies found that holding the vesicles close together for tens of nanoseconds was sufficient to cause fusion. Stevens *et al.* studied⁷⁹ the fusion of two vesicles containing about 1000 lipids that were pushed together by the application of a transient force to all membrane molecules. The force was removed after a few lipids had exchanged between the vesicles, and the subsequent fusion processes were followed for hundreds of microseconds. Fusion appeared to start at the edge of the flattened contact zone between the two vesicles, where the curvature of the surface is greatest. The stalk in these fusion events was found to expand asymmetrically around the strained edge of the contact zone leading to a partially-confined solvent cavity between the two vesicles. This results in the fusion pore typically forming at points distant from the point of closest approach of the vesicles. In the simulations of Marrink *et al.*,^{80,81} the vesicles were held a fixed distance apart until the lipids started to mix. The initial contact between the vesicles was provided by a few lipids whose protrusion fluctuations caused them to merge into the apposed monolayer. They found that successful fusion depended on the lipid species in the vesicles⁸⁰: mixtures of dipalmitoylphosphatidylcholine (DPPC) and palmitoyl-oleoyl phosphatidylethanolamine (POPE) fused most easily at separations up to 1.5 nm; vesicles composed of pure DPPC only fused when held closer together than 1 nm for more than 50 ns; and vesicles containing DPPC and 25% lysoPC were not seen to fuse at all within 200 ns. Although limited in their spatial scope by available computing resources, coarse-grained⁸¹ and atomistic⁸² MD simulations reveal unprecedented detail on the molecular rearrangements in membranes during phase transitions, such as the formation of a hexagonal phase. The latter work⁸² showed that stalks connecting lamellae form spontaneously as the initial gel phase lipids transform into an inverted hexagonal phase.

The high curvature of the vesicles in these MD simulations (each of which is approximately 15 nm in diameter) may influence their fusion pathway, and larger vesicles would be a better model for experimental systems such as synaptic vesicle fusion in which vesicles of 40 nm diameter take part. The fusion of two closely-apposed, tense *planar* membrane patches composed of amphiphilic copolymers has

been studied using canonical ensemble, lattice Monte Carlo simulations⁸³ in three dimensions. The size ratio of the hydrophilic to hydrophobic parts (11 segments and 21 segments respectively) is chosen to be close to that appropriate to biological lipids. The solvent is a homopolymer. The molecules in these simulations do not obey Newtonian dynamics, but evolve according to a Markov process (using the Metropolis² algorithm) that ensures the correct statistical weight for states of the system in equilibrium. Ensemble averages then provide the connection with physical properties. Because the total densities of each segment type are conserved, the motion of the polymers is diffusive.

Contacts between the molecules in the membranes arise naturally in this model as a result of thermal shape fluctuations. Most of these contacts rapidly disappear, but some lead to formation of a “stalk” or merging of regions of the closest (cis) monolayers. Once a stalk has formed, the probability of a hole appearing in one or other bilayer near the stalk increases markedly. The presence of the nearby hole then appears to encourage the stalk to traverse around it and form a ring-like connection between the membranes. The authors explain the increased probability of hole formation close to a stalk as the result of a lowering of the line tension around such a hole caused by the reduction in the curvature of the piece of membrane between the hole and the stalk. The final stage in the observed fusion process is the appearance of a second hole in the other membrane and the movement of the stalk to surround both holes. This results in the full fusion pore connecting the distal sides of the membranes. Similar results were observed in Self-Consistent Field Theory (SCFT) simulations⁸⁴ of large systems of symmetric, amphiphilic diblock copolymers, including the formation of a pore close to the stalk connecting two fusing membranes. Recent work⁸⁵ on a similar model using SCFT methods emphasizes the key role of line tension in this model of membrane fusion.

The key steps leading to membrane fusion are: close proximity of the two membranes; initial contact and inter-penetration of the outer leaflets; opening of a pore connecting both membranes; and release of the vesicle contents. In order to get closer to the experimental length scale for synaptic vesicles, we have recently studied¹⁴ the tension-induced fusion of a 28 nm diameter vesicle to a $50 \times 50 \text{ nm}^2$ planar membrane patch using DPD simulations. We focus on the molecular rearrangements that occur after the initial contact of the two fusing membranes, and use the global tension in the membranes as the control parameter. Increasing the tension in a membrane eventually results in its rupture. If an alternative pathway is possible, such as merging with a closely-apposed, less tense membrane, the rupture end-point can be avoided. In these simulations, the relaxed vesicle contains approximately 6,500 lipids, and the relaxed planar membrane contains around 8,200 lipids. These are an order of magnitude larger than any published atomistic, or coarse-grained, Molecular Dynamics fusion study. We note here that the membranes used in this study are significantly more stretchable than typical lipid membranes, and are more similar in this respect to those formed of diblock copolymers. This may influence the time-scale over which the fusion pore opens up, and partially explain

the difference between the hundreds of nanoseconds required for fusion in the simulations and the hundreds of microseconds estimated from experiments⁶⁷. However, the model system captures the features that we believe are important for understanding the molecular rearrangements that occur during the fusion of tense membranes. The global tensions in the vesicle and planar membrane are created by appropriately choosing the number of molecules in each membrane. Repeating the protocol for each tension pair, using thermodynamically equivalent, but molecularly distinct, initial states, allows the probabilities of the various outcomes to be obtained. A typical fusion event proceeds as follows. After the initial membrane contact there is a rapid transfer of molecules from the (more relaxed) vesicle to the cis leaflet of the (more tense) planar membrane which destabilizes the merged contact zone, and leads to the fusion pore, which subsequently enlarges rapidly due to the larger tension in the membrane. For more details, the reader is referred to the original paper.¹⁴

Successful fusion events were only observed in these simulations for membrane and vesicle tensions not far from values that caused their spontaneous rupture. Lower tensions resulted in the adhesion or hemifusion of the vesicle to the planar membrane. Secondly, successful fusion events all occurred between 150 and 350 ns after initial contact of the two membranes even though the simulations were run out to almost 2 microseconds. The fusion time is defined here as the simulation time between the first contact of the two membranes, and the time when the pore has expanded approximately to the diameter of the vesicle. These times are consistent with the extrapolation of recent experimental studies⁶⁸ of controlled fusion of vesicles. The upper cut-off of the fusion time distribution arises from the stabilization of the hemifused state in the membrane geometry used here. Because the hemifused state is metastable for relatively large initial tensions, fusion can occur only at even higher tensions for which the fusion pathway exhibits no activation barrier. The stabilization of the hemifused state depends on the membrane areas that are initially stretched: if the vesicle and planar membrane areas are comparable, the planar membrane can relax its (higher) tension by incorporating vesicle lipids before a fusion pore can appear. If the planar membrane area is much larger than the vesicle area, the hemifused states are only stabilized for smaller initial tensions, and the region of successful fusion is shifted towards smaller tensions.

In these DPD simulations, one can measure the functional dependence of the membrane tension on the projected area per molecule up to the tension of rupture as observed within about $10 \mu\text{s}$. For the DPD parameters used in Refs. 9 and 14, this functional relationship between tension and molecular area is rather non-linear, and the membrane becomes more and more compressible as it is stretched. Varying the DPD parameters in a systematic manner, we have identified parameter sets for which the functional dependence between tension and molecular area is fairly linear^{86,87}. For the parameter set in Ref. 87, we have observed a strong increase in the fusion time with decreasing tension, which implies a tension-dependent energy barrier for the fusion process.

Vesicle fusion *in vivo* requires the participation of proteins, such as the SNARE proteins that cause synaptic vesicle fusion in neurons. A more realistic fusion protocol is to embed model proteins in relaxed membranes, and to explore their possible actions in driving the membranes to fuse. Several groups are exploring how to embed peptides or proteins into simulated membranes using atomistic^{88,89} and coarse-grained⁹⁰ MD, and DPD,^{6,53} The challenge for these groups is to integrate the results of different simulation techniques into an understanding of the complete fusion process from the molecular rearrangements occurring on the microscopic scale to the time course of the fusion pore conductivity on physiological length and time scales.

5. Nanoparticles and Vesicles

Interest in the development of rigid nanoparticles and layered capsules has grown as these substances have found application as anti-tumor devices,^{17,91} and as drug delivery vehicles.^{4,15} This has resulted in a need to understand and optimize their properties for specific purposes. DPD has previously been used to simulate colloidal systems,^{30,49} and recently also the flow of fluid through microchannels.⁹² The latter ability may be useful in developing models for clinical applications of microfluidics.⁹³ An important potential application involves the interactions between flexible polymers and quantum dots. Quantum dots are a class of nanoparticles whose preparation and growth properties⁵ are still incompletely understood. Experimental manipulation of quantum dots can involve transferring them from non-polar solvents into water, and using amphiphilic, hyperbranched polymers to prevent their aggregating in the water.⁹⁴ Exploring the interactions of amphiphilic polymers with the quantum dots' hydrophobic surfaces is an interesting target system for DPD. In this section we describe the first step to understanding the dynamics of rigid nanoparticles in DPD by quantifying the bulk diffusion of non-aggregating, rigid, colloidal particles embedded in a solvent. This system may be useful in modeling the motion of globular proteins in fluid, or rigid drug delivery vehicles such as polymerised capsules.

Dissipative Particle Dynamics has mainly been applied to the study of fluid systems, as this is the field in which it was originally developed. There have been a few publications describing quasi-rigid peptides embedded in a lipid membrane,⁵³ the flow behavior of fluids at solid surfaces,²⁸ the interaction of colloidal particles in a solvent,⁹⁵ and the derivation of the DPD equations from first principles for a one-dimensional harmonic solid,⁹⁶ but these are the exception. In keeping with the spirit of DPD, in which the forces are soft and short-ranged, we construct a "rigid" particle embedded in a solvent by selecting all the solvent beads whose centre of mass coordinates lie within a specified geometric volume (either a cylinder, sphere or an ellipsoid), and tying them together with stiff Hookean springs. Hereafter, we refer to such a "polymerised particle" as a *nanoparticle* to distinguish it from the

spherical DPD solvent particles. By choosing the spring parameters appropriately, the rigidity of the nanoparticle can be tuned within a fairly wide range. A simple measure of rigidity is given by the fluctuations of the average shape of the particle: a rigid particle has only small-amplitude shape fluctuations whereas a less rigid nanoparticle has larger shape fluctuations. We are interested in simulating the interactions between nanoparticles, membranes and bulk solvents, so an appropriate criterion for their rigidity is that the fluctuations in the size of the nanoparticles should be less than a few percent of their mean size. This ensures that they interact with the surrounding soft fluids as a relatively hard object.

The first test we have performed on the nanoparticles is to measure their diffusion in a bulk solvent. Because a DPD fluid correctly represents hydrodynamic forces,^{7,8} we expect that the diffusion of such particles should obey Stokes' law, which states that the diffusion coefficient of a spherical particle (D) varies inversely with its radius (R):

$$D = \frac{k_B T}{6 \pi \eta R} \quad (6)$$

where η is the solvent viscosity, k_B is Boltzmann's constant, and T is the temperature. The mean-square displacement (MSD) of a single nanoparticle is a three-dimensional random walk, and in order to obtain a statistically-significant result for small particles, we average the MSD over four independent trajectories. The larger particle's trajectory showed smaller fluctuations so a single trajectory is used. However, because of the long-range hydrodynamic forces, the larger particles must be simulated in a box with linear dimensions $48 * d_0$, while the smaller particle was simulated in one with dimensions $32 * d_0$.

Figure 2 shows the mean-square displacement (MSD) of rigid, spherical nanoparticles with radius $R/d_0 = 2$ and 4 normalised by the elapsed time as a function of the simulation time. The ratio of the y intercepts of the two curves is very close to the ratio of their radii, showing that the diffusion of the nanoparticles does obey Stokes law, at least for the particle sizes chosen. We note here that there are practical limits to the sizes of rigid particles that can be accurately represented in a DPD simulation. If the diffusing particle is comparable in size to the surrounding solvent particles, the assumption of random independent collisions of the fluid on the particle no longer holds. At the other extreme, a large diffusing particle is subject to hydrodynamic forces whose range is many times the size of the particle, and can be larger than the simulation box (except for extremely large boxes whose investigation would waste computer resources in simulating a system that is almost entirely solvent). Even for particles with a radius only four times the solvent bead diameter, $R/d_0 = 4$, we were obliged to use a larger simulation box than for the smaller particle. The calculation of each trajectory for the small particle required 5 cpu-days on a single-processor 2 GHz Xeon processor, whereas the larger particle trajectory required 17.5 cpu-days.

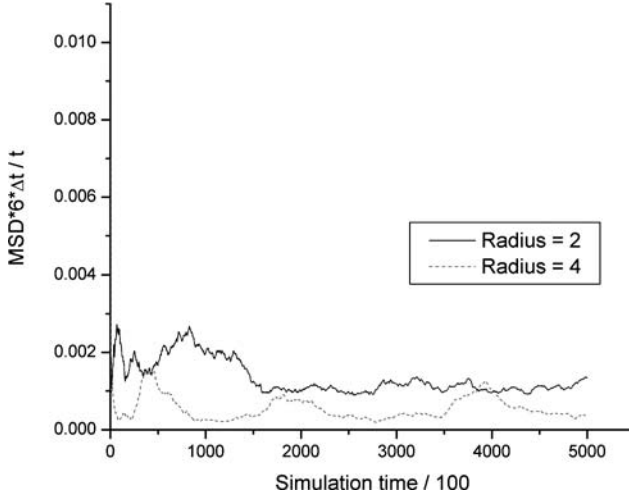


Fig. 2. Ratio of the mean-square displacement (MSD) to the elapsed time for freely-diffusing nanoparticles with radii $R = 2 * d_0$ and $4 * d_0$ in bulk solvent versus the simulation time (Note that the y-axis values must be divided by the constant term $6 * \Delta t$, where $\Delta t = 0.01$ is the integration time-step in order to obtain the actual ratio; the x-axis values are the number of time-steps elapsed). Each nanoparticle is constructed out of a sphere of solvent beads that are “tied” together using stiff Hookean springs as described in the text. The curve for the smaller particle is an average over 4 independent runs, whereas the curve for the larger particle is for a single run. Because the total force on a nanoparticle is the sum over the forces acting on its surface, and momentum is conserved by the DPD interactions, the long-range hydrodynamic forces mediated by the solvent are present. This requires the use of a simulation box with linear dimension $48 * d_0$ for the $D = 4 * d_0$ particle as smaller box sizes showed artificially damped diffusion due to the periodic images of the nanoparticle. The smaller particle was simulated in a box with linear dimension $32 * d_0$. We calculate the diffusion constants of the nanoparticles by fitting the data between 200,000 and 500,000 time steps to a straight line of zero slope and taking the intercept on the y axis. This gives values of $D = 0.0005 \pm 0.0001$ and $D = 0.0011 \pm 0.00005$ for the larger and smaller nanoparticles respectively (the quoted standard deviation is for statistical errors only, and the correlations between successive data points are removed by binning the data into three groups and calculating the standard deviation of the groups’ mean values).

The interaction of rigid nanoparticles with soft surfaces is relevant to clinically-important processes such as virus envelopment by cell membranes,⁹⁷ and the practical problems of translocation of nanoparticles through a liquid-liquid interface.⁹⁸ A theoretical analysis⁹⁹ of the interaction between spherical nanoparticles and vesicles revealed different situations that depended on whether the particles were repelled from the membrane or attracted to it, and on the particle size. Such processes are amenable to investigation using DPD. We have performed simulations in which four nanoparticles, whose diameter of 4 nm is comparable to the membrane thickness, are constructed out of fluid beads inside a vesicle’s lumen using the above protocol. The surface of the nanoparticles can be hydrophilic or hydrophobic. They diffuse freely inside the vesicle until they encounter the membrane’s inner surface. If the nanoparticles’ surface is hydrophilic they wrap themselves in the membrane causing it to bulge outwards, as illustrated in Fig. 3. This is similar to recent theoretical¹⁰⁰

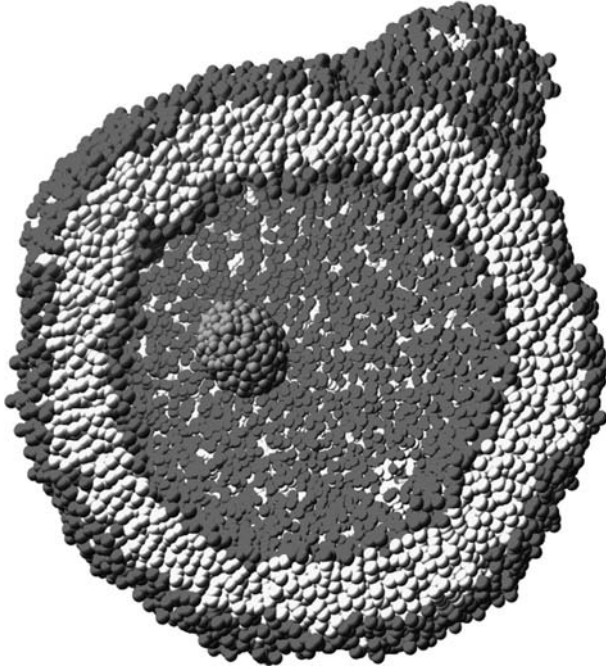


Fig. 3. A cut through a vesicle with diameter 28 nm containing four small, rigid nanoparticles each approximately 4 nm in width. The surfaces of the nanoparticles are hydrophilic, and their conservative interaction parameters are chosen so that they tend to adhere to the vesicle membrane when they encounter it. As the membrane wraps around a nanoparticle, it tends to bulge outwards in a process that is similar to the initial stage of budding of the vesicle membrane. Only one of the nanoparticles is clearly visible in the vesicle lumen in this image, a second is wrapped in the membrane producing the large bulge at the upper right, and the other two are embedded in the membrane at the top left and bottom right of the image, and are hidden by the perspective. Although not obvious in a static image, the rigidity of the nanoparticles is such that their shape fluctuations are smaller than one DPD bead diameter. (Image produced using the PovRay ray tracing program: www.povray.org.)

and Molecular Dynamics simulation¹⁰¹ studies of a colloidal particle being wrapped by a membrane. Hydrophobic nanoparticles burrow into the membrane's hydrophobic core where they cause the membrane to bulge around them. Figure 3 shows a cut through the vesicle showing the hydrophilic nanoparticles partially wrapped in the vesicle membrane. Adhesion of nanoparticles to membranes, and their subsequent budding off, has also been studied using Brownian Dynamics simulations.¹⁰² The ability to study a process using different simulation methodologies is important to avoid the bias that may be present in a single technique. Additionally, the incorporation of hydrodynamic forces in DPD, which are absent in Brownian Dynamics and solvent-free simulations, may be important in the *in vivo* flow environment of cells in the human body. Such forces may play an important role in the approach of globular proteins and drug molecules to cell membrane receptors.³

6. Conclusions and Outlook

DPD allows fluid systems with hydrodynamics to be simulated and visualized. For certain systems, such as polymeric fluids and amphiphilic membranes, it can provide quantitative information similar to that available from coarse-grained Molecular Dynamics simulations. In particular, quantities such as the lateral stress profile and elastic moduli of fluid membranes can be measured. Many groups are now applying DPD to diverse systems, such as lipid membranes,^{10–12} diblock copolymer vesicles,¹³ fusion of vesicles to planar membrane patches,¹⁴ surface-grafted polymer brushes,^{34,103} colloidal micropumps,⁹² and models of protein fragments that are implicated in the development of Huntington’s disease.⁵¹ The range of applications will doubtless grow further over the next few years. The incorporation of movable, rigid particles into DPD simulations, such as transmembrane proteins,^{6,53} whilst retaining the benefits of a larger time-step than coarse-grained MD, is an important advance of the method.

Nanoparticles are used in various processes including ones important for the development of effective therapeutic agents,^{4,16,17} and the construction⁵ of Quantum Dots. The construction of such nanoparticles requires that their growth be accurately characterized and controllable. Visualizing the effects of changes in growth conditions on the evolution of the nanoparticles provides important feedback for optimizing the growth process. We have begun to validate the behavior of rigid nanoparticles in a DPD simulation by verifying the Stokes’ drag relation between particle size and diffusion for small particles. We have also shown that nanoparticles can adsorb to, and be wrapped by, a vesicle membrane. This opens the way to using mesoscopic simulations to explore the interactions of nanoparticles, membranes, and other soft materials, and developing a systematic method for quantifying their properties in support of experimental efforts to create useful new materials. A promising application of these simulations is the interaction between nanoparticles and the proteins involved in cell signaling networks. The clinical use of designed nanoparticles requires understanding their biophysical behavior and the ability to minimize their toxic effects. We conclude with our vision of how mesoscopic simulations may aid in the development of our understanding of, and our ability to rationally modify, cell signaling networks.

Cell signaling networks combine the various topics we have discussed in this article. They are important as targets for therapeutic intervention in disease detection and control. The ability to simulate the cellular uptake of a drug, and its modulated response when either the drug or its delivery mechanism are modified, are recognised as crucial to future drug development.³ It is not possible to capture a signaling network in a single type of simulation because of the huge range of relevant length and time scales. These encompass the nanometer width of the plasma membrane and the ten-micron size of the cell, and span nanoseconds to seconds or longer. A combination of techniques is therefore required that each captures some of the key stages in the signaling process. Figure 4 illustrates the division of a generic cellular signaling process into three spatio-temporal regions: the plasma

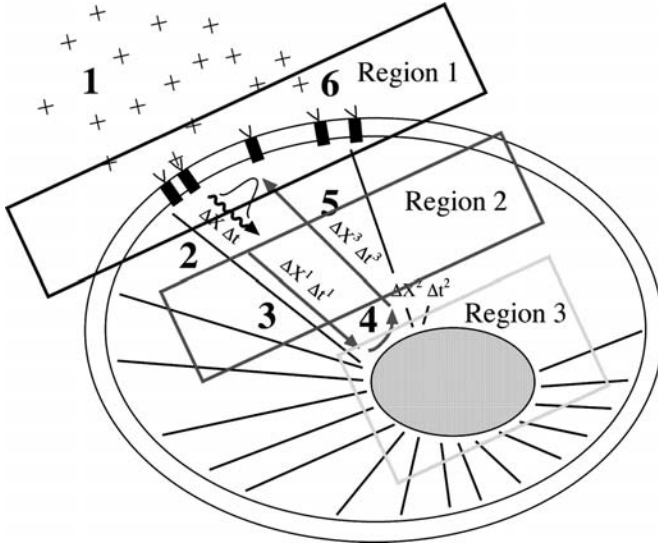


Fig. 4. Illustration of one possible division of a cellular signaling pathway model into three regimes suitable for modeling using different simulation methods. The numbers 1–6 in bold type refer to distinct transduction mechanisms relevant to the pathway as described in the text. Region 1 has length and time scales of ~ 100 nm and a few microseconds and can be modeled using a coarse-grained Molecular Dynamics or Dissipative Particle Dynamics method. This regime captures the diffusion of ligands or other extracellular messengers (represented by small crosses) to the plasma membrane and their binding to transmembrane receptors (solid cylinders). Region 2 has a length scale of approximately the size of the cell (5–10 microns) and the transport of secondary messengers or transport vesicles through this region could be simulated using Brownian Dynamics or a similar, solvent-free method. Region 3 represents the process of control of gene expression resulting from the receipt of the signal at the nucleus. Modeling of this stage is still speculative, but analytic models could provide useful insight.

membrane (Region 1), the cytoplasmic space (Region 2) and the near-nuclear space (Region 3). Within these regions, we identify distinct space-time envelopes for the propagation of the signal (represented by the symbols Δx , Δt , and labelled 1 to 3 in Fig. 4), each of which provides opportunities for therapeutic intervention that can be explored by appropriate simulation techniques. First, a signal is carried from the extra-cellular space to the cell by diffusion of ligands to membrane-bound receptors (1) In this stage hydrodynamic forces may be important as the (possibly bulky) ligands approach and bind to, and/or occlude, the receptors. Second, the signal is transduced across the plasma membrane (2) A variety of membrane-associated processes influence this stage. For example, receptors may cluster in the plasma membrane so as to magnify the initial ligand-induced signal, followed by endocytosis of the activated receptors. The fluid character of the membrane, and the inplane diffusion of the receptors are key properties here. Next a network of protein-protein interactions integrates the signal and propagates it through the cytoplasm (3) to its destination organelle(s). For many signals this is the nucleus, where the cell's pattern of gene expression is modified (4) in response to the signal. The cytoskeleton

of the cell may be closely involved in this stage of signal propagation.^{104,105} Finally, the response of the cell to the signal occurs, possibly involving new protein creation and transportation (5) and up- or down regulation of existing transmembrane proteins (6).

Each stage of this signaling process may be captured in a distinct simulation type. Region 1 occupies perhaps a 100 nm space around the plasma membrane, and is suitable for simulating using DPD or coarse-grained MD which can reach the required microsecond time-scale. The cytoplasmic space, Region 2, is too large for current explicit-solvent models with near-molecular detail, but may be adequately represented using Brownian Dynamics or spatially-inhomogeneous stochastic differential equations. Region 3 includes the modification of the cell's gene expression, and its representation and coupling to the other transmission processes will probably also involve a coupled set of stochastic differential equations. Each region provides distinct opportunities for exploring, and then optimizing, modifications to the signaling machinery. Drug molecules or artificial nanoparticles may interfere with the initial ligand binding;³ the signaling cascades may be changed by modifying the proteins composing them;¹⁰⁶ and protein-protein interactions may be made visible by use of self-illuminating Quantum Dots.¹⁰⁷ The ability to simulate on realistic length and time scales key biophysical processes such as vesicle fusion, artificial drug delivery vehicles, and the interaction of rigid nanoparticles with fluid membranes, opens the way to systematically constructing models of cellular signaling processes. These models will assist in optimizing the interactions between artificial materials and the cellular machinery that is the target of therapeutic intervention.

We believe that mesoscopic simulations provide a natural complement to the experimental task of rationally constructing biomimetic materials, and that simulations can act as a *lingua franca* between experimental groups using very different techniques. The results of thousands of experiments can be efficiently represented in simulation models, and communicated accurately between groups, thereby expanding the usefulness of such models from computational biology to the larger fields of biophysics and clinical biology.

Acknowledgments

One of the authors (JCS) gratefully acknowledges funding from the Human Frontier Science Project under the grant: "Signaling to actin: from cell movement to biomimetic motile systems."

References

1. B. J. Alder and T. E. Wainwright, *J. Chem. Phys.* **27**, 1208 (1957).
2. N. Metropolis, A. W. Rosenbluth, M. N. Rosenbluth, A. H. Teller and E. Teller, *J. Chem. Phys.* **21**, 1087 (1953).

3. B. M. Rao, D. A. Lauffenburger and K. D. Wittrup, *Nature Biotechnology* **23**, 191 (2005).
4. E. Mastrobattista, M. A. E. M. van der Aa, W. E. Hennink and D. J. A. Crommelin, *Nature Reviews Drug Discovery* **5**, 115 (2006).
5. S. Kumar and T. Nann, *Small* **2**, 316 (2006).
6. J. C. Shillcock and R. Lipowsky, *J. Phys.: Condens. Matter* **18**, S1191 (2006).
7. P. J. Hoogerbrugge and J. M. V. A. Koelman, *Europhys. Lett.* **19**, 155 (1992).
8. P. Espagnol and P. Warren, *Europhys. Lett.* **30**, 191 (1995).
9. J. C. Shillcock and R. Lipowsky, *J. Chem. Phys.* **117**, 2048 (2002).
10. M. Kranenburg, M. Vlaar and B. Smit, *Biophys. J.* **87**, 1596 (2004).
11. G. Illya, R. Lipowsky and J. C. Shillcock, *J. Chem. Phys.* **122**, 244901 (2005).
12. G. Illya, R. Lipowsky and J. C. Shillcock, *J. Chem. Phys.* **125**, 114710 (2006).
13. V. Ortiz, S. O. Nielsen, D. E. Discher, M. L. Klein, R. Lipowsky and J. C. Shillcock, *J. Phys. Chem. B* **109**, 17708 (2005).
14. J. C. Shillcock and R. Lipowsky, *Nature Mater.* **4**, 225 (2005).
15. H. Rosen and T. Aribat, *Nature Reviews Drug Discovery* **4**, 381 (2005).
16. R. Weissleder, K. Kelly, E. Y. Sun, T. Shtatland and L. Josephson, *Nature Biotechnology* **23**, 1418 (2005).
17. S. Sengupta, D. Eavarone, I. Capila, G. Zhao, N. Watson, T. Kiziltepe and R. Sasisekharan, *Nature* **436**, 568 (2005).
18. D. W. Pack, A. S. Hoffman, S. Pun and P. S. Stayton, *Nature Reviews Drug Discovery* **4**, 581 (2005).
19. V. P. Torchilin, *Nature Reviews Drug Discovery* **4**, 145 (2005).
20. T. M. S. Chang, *Nature Reviews Drug Discovery* **4**, 221 (2005).
21. G. B. Sukhorukov, A. Fery and H. Möhwald, *Prog. Polym. Sci.* **30**, 885 (2005).
22. G. B. Sukhorukov, A. L. Rogach, B. Zebli, T. Liedl, A. G. Skirtach, K. Köhler, A. A. Antipov, N. Gaponik, A. S. Susha, M. Winterhalter and W. J. Parak, *Small* **1**, 194 (2005).
23. R. D. Groot and P. B. Warren, *J. Chem. Phys.* **107**, 4423 (1997).
24. P. B. Warren, *Curr. Op. Coll. Interface Sci.* **3**, 620 (1998).
25. J. C. Shelley and M. Y. Shelley, *Curr. Op. Coll. Interface Sci.* **5**, 101 (2000).
26. M. Kranenburg, J.-P. Nicolas and B. Smit, *Phys. Chem. Chem. Phys.* **6**, 4142 (2004).
27. R. D. Groot and T. J. Madden, *J. Chem. Phys.* **20**, 8713 (1998).
28. J. L. Jones, M. Lal, J. N. Ruddock and N. A. Spensley, *Faraday Discuss.* **112**, 129 (1999).
29. R. D. Groot, *Langmuir* **16**, 7493 (2000).
30. M. Whittle and E. Dickinson, *J. Coll. Interface Sci.* **242**, 106 (2001).
31. R. D. Groot and K. L. Rabone, *Biophys. J.* **81**, 725 (2001).
32. L. Rekvig, M. Kranenburg, J. Vreede, B. Hafskjold and B. Smit, *Langmuir* **19**, 8195 (2003).
33. P. Prinsen, P. B. Warren and M. A. J. Michels, *Phys. Rev. Lett.* **89**, 148301 (2003).
34. D. Irfachsyad, D. Tildesley and P. Malfreyt, *Phys. Chem. Chem. Phys.* **4**, 3008 (2002).
35. S. D. Stoyanov and R. D. Groot, *J. Chem. Phys.* **122**, 114112 (2005).
36. T. Soddemann, B. Dunweg and K. Kremer, *Phys. Rev. E* **68**, 046702 (2003).
37. G. Besold, I. Vattulainen, M. Karttunen and J. M. Polson, *Phys. Rev. E* **62**, 7611 (2000).
38. P. Nikunen, M. Karttunen and I. Vattulainen, *Comp. Phys. Comm.* **153**, 407 (2003).
39. A. F. Jakobsen, *J. Chem. Phys.* **122**, 124901 (2005).
40. C. P. Lowe, *Europhys. Lett.* **47**, 145 (1999).

41. E. A. J. F. Peters, *Europhys. Lett.* **66**, 311 (2004).
42. W. K. den Otter and J. H. R. Clark, *Europhys. Lett.* **53**, 426 (2001).
43. P. B. Warren, *Phys. Rev. Lett.* **87**, 225702 (2001).
44. T. Shardlow, *SIAM J. Sci. Comput. (USA)* **24**, 167 (2003).
45. A. F. Jakobsen, O. G. Mouritsen and G. Besold, *J. Chem. Phys.* **122**, 204901 (2005).
46. R. Goetz and Lipowsky, *J. Chem. Phys.* **108**, 7397 (1998).
47. M. Venturoli and B. Smit, *Phys. Chem. Comm.* **10**, 1 (1999).
48. A. Imparato, J. C. Shillcock and R. Lipowsky, *Europhys. Lett.* **69**, 650 (2005).
49. M. Laradji and M. J. A. Hore, *J. Chem. Phys.* **121**, 10641 (2004).
50. H.-J. Qian, Z.-Y. Lu, L.-J. Chen, Z.-S. Li and C.-C. Sun, *J. Chem. Phys.* **122**, 184907 (2005).
51. M. G. Burke, R. Woscholski and S. N. Yaliraki, *PNAS* **100**, 13928 (2003).
52. V. Symeonidis, G. E. Karniadakis and B. Caswell, *Phys. Rev. Lett.* **95**, 076001 (2005).
53. M. Venturoli, B. Smit B and M. M. Sperotto, *Biophys. J.* **88**, 1778 (2005).
54. S. Yamamoto, Y. Maruyama and S. Hyodo, *J. Chem. Phys.* **116**, 5842 (2002).
55. S. Yamamoto and S. Hyodo, *J. Chem. Phys.* **118**, 7937 (2003).
56. M. Laradji and P. B. S. Kumar, *J. Chem. Phys.* **123**, 224902 (2005).
57. M. Antonietti and S. Förster, *Adv. Mater.* **15**, 1323 (2003).
58. L. F. Zhang, K. Yu and A. Eisenberg, *Science* **272**, 1777 (1996).
59. B. M. Discher, Y.-Y. Won, D. S. Ege, J. C.-M. Lee, F. S. Bates, D. E. Discher and D. A. Hammer, *Science* **284**, 1143 (1999).
60. F. Meng, G. H. M. Engbers and J. Feijen, *J. Controlled Release* **101**, 187 (2005).
61. A. Napoli, M. Valentini, N. Tirelli, M. Müller and J. A. Hubbell, *Nature Mater.* **3**, 183 (2004).
62. K. Vijayan, D. E. Discher, J. Lal, P. Janmey and M. Goulian, *J. Phys. Chem. B* **109**, 14356 (2005).
63. Y. Zhou and D. Yan, *J. Am. Chem. Soc.* **127**, 10468 (2005).
64. G. Srinivas, D. E. Discher and M. L. Klein, *Nature Mater.* **3**, 638 (2004).
65. V. Kiessling, *Biophys. J.* **89**, 2185 (2005).
66. T. Liu, W. C. Tucker, A. Bhalla, E. R. Chapman and J. C. Weisshaar, *Biophys. J.* **89**, 2458 (2005).
67. M. Lindau and G. A. de Toledo, *Biochim. Biophys. Acta.* **1641**, 167 (2003).
68. C. K. Haluska, K. A. Riske, V. Marchi-Arztner, J.-M. Lehn, R. Lipowsky and R. Dimova, *PNAS* **103**, 15841 (2006).
69. A. Mayer, *Ann. Rev. Cell Dev. Biol.* **18**, 289 (2002).
70. R. Jahn and H. Grubmüller, *Curr. Op. Cell Biol.* **14**, 488 (2002).
71. R. Jahn, T. Lang and T. Südhof, *Cell* **112**, 519 (2003).
72. L. K. Tamm, J. Crane and V. Kiessling, *Curr. Op. Struct. Biol.* **13**, 453 (2003).
73. C. Ungermann and D. Langosch, *J. Cell Science* **118**, 3819 (2005).
74. L. V. Chernomordik and M. L. Kozlov, *Cell* **123**, 375 (2005).
75. G. Lei and R. C. Macdonald, *Biophys. J.* **85**, 1585 (2003).
76. F. Nomura, T. Inaba, S. Ishikawa, M. Nagata, S. Takahashi, H. Hotani and K. Takiguchi, *PNAS* **101**, 3420 (2004).
77. M. Fix, T. J. Melia, J. K. Jaiswal, J. Z. Rappoport, D. You, T. H. Söllner, J. E. Rothman and S. M. Simon, *PNAS* **101**, 7311 (2005).
78. P. M. Kasson, N. W. Kelley, N. Singhal, M. Vrljic, A. T. Brunger and V. S. Pande, *PNAS* **103**, 11916 (2006).
79. M. J. Stevens, J. H. Hoh and T. B. Woolf, *Phys. Rev. Lett.* **91**, 188102 (2003).
80. S.-J. Marrink and A. E. Mark, *J. Am. Chem. Soc.* **125**, 11144 (2003).
81. S.-J. Marrink and A. E. Mark, *Biophys. J.* **87**, 3894 (2004).

82. V. Knecht, A. E. Mark and S.-J. Marrink, *J. Am. Chem. Soc.* **128**, 2030 (2006).
83. M. Müller, K. Katsov and M. Schick, *Biophys. J.* **85**, 1611 (2003).
84. G. J. A. Sevink and A. V. Zvelindovsky, *Macromolecules* **38**, 7502 (2005).
85. M. Schick, K. Katsov and M. Müller, *Molecular Physics* **103**, 3055 (2005).
86. L. Gao, R. Lipowsky and J. C. Shillcock, *J. Chem. Phys.* (in press 2007).
87. A. Grafmüller, R. Lipowsky and J. C. Shillcock (in preparation).
88. C. Appelt, F. Eisenmenger, R. Kühne, P. Schmieder and J. A. Söderhäll, *Biophys. J.* **89**, 2296 (2005).
89. L. Saiz and M. L. Klein, *Biophys. J.* **88**, 959 (2005).
90. G. Srinivas, C. F. Lopez and M. L. Klein, *J. Phys. Chem. B* **108**, 4231 (2004).
91. M. Ferrari, *Nature Reviews Cancer* **5**, 161 (2005).
92. P. De Palma, P. Valentini and M. Napolitano, *Physics of Fluids* **18**, 027103 (2006).
93. P. S. Dittrich and A. Manz, *Nature Reviews Drug Discovery* **5**, 210 (2006).
94. T. Nann, *Chem. Commun.* 1735 (2005).
95. E. S. Boek, P. V. Coveney and H. N. W. Lekkerkerker, *J. Phys.: Condens. Matter* **8**, 9509 (1996).
96. P. Espagnol, *Phys. Rev. E* **53**, 1572 (1996).
97. S. X. Sun and D. Wirtz, *Biophys. J.* **90**, L10 (2006).
98. L. Livadaru and A. Kovalenko, *Nanoletters* **6**, 78 (2006).
99. R. Lipowsky and H.-G. Döbereiner, *Europhys. Lett.* **43**, 219 (1998).
100. M. Deserno, *Phys. Rev. E* **69**, 031903 (2004).
101. I. R. Cooke and M. Deserno, *Biophys. J.* **91**, 487 (2006).
102. H. Noguchi and M. Takasu, *Biophys. J.* **83**, 299 (2002).
103. S. Pal and C. Seidel, *Macromolecular Theory and Simulations* **15**, 668 (2006).
104. P. A. Janmey, *Physiological Review* **78**, 763 (1998).
105. G. Forgacs, S. H. Yook, P. A. Janmey, H. Jeong and C. G. Burd, *J. Cell Science* **117**, 2769 (2004).
106. S.-H. Park, A. Zarrinpar and W. A. Lim, *Science* **299**, 1061 (2003).
107. M.-K. So, C. Xu, A. M. Loening, S. S. Gambhir and J. Rao, *Nature Biotechnology* **24**, 339 (2006).